Blind Motion Compensation for Positron-Emission-Tomography

Moritz Blume[a,b], Andreas Keil[b], Nassir Navab[b], Magdalena Rafecas[a]

[a]Instituto de Física Corpuscular, Edificio Institutos de Investigación Polígono de la Coma, E-46980 Paterna, Spain

[b]Computer Aided Medical Procedures, Fakultät für Informatik, Technische Universität München, Boltzmannstr. 3, 85748 Garching bei München, Germany

ABSTRACT

A major problem of high-resolution positron-emission-tomography (PET) are subject movements during acquisition. We propose a new motion compensation algorithm called "Blind Motion-Compensated Reconstruction" (BMCR) that is able to deal with frames of extremely low statistics in the case of smooth motion. Our algorithm reconstructs both image and rigid motion just from the recorded data and does not need any external motion tracking.

This is achieved by combining image reconstruction and motion compensation into one mathematical framework which consists of a cost functional and an optimization method. The cost functional basically consists of a difference term which ensures consistency of the estimated parameters to the model and some regularization terms which render the problem mathematically well-posed. The optimization method aims at finding a pair of image and transformation/motion such that the cost functional is minimal.

Such a combined framework can overcome problems of existing algorithms which separate reconstruction and motion compensation. These algorithms usually try to get the motion information by registering reconstructed frames one to each other (in image space). Their main drawback is that the registration step is likely to be of low accuracy or even fail completely for low-statistics frames.

A quantitative and visual comparison suggests that BMCR is superior to state-of-the-art intrinsic methods.

Keywords: PET, reconstruction, motion-compensation, intrinsic, blind

1. INTRODUCTION

Motion compensation algorithms for PET can be roughly divided into two categories: Those which try to get the motion information from the data itself (*intrinsic*), and those that use additional methods like optical tracking to acquire the motion information (*extrinsic*).

Existing *intrinsic* algorithms usually separate reconstruction and motion compensation: They first perform a reconstruction of each frame and then try to get the motion information by registering one to each other (in image space). Finally, they either combine the reconstructed frames by some weighting/averaging[1] or use all statistical information for reconstruction.[2,3] We call this class of methods registration-and-fusion-of-reconstructed-frames methods (RFRF).

The registration step is crucial: On the one hand, time frames have to be short and therefore numerous in order to assure low intra-frame motion. On the other hand, short time frames only dispose of few statistical information and thus result in noisy images which are extremely difficult to register.

The paper is organized as follows: In section 2.1 we propose our new motion-compensation algorithm BMCR. Section 2.2 explains our implementation of the RFRF method. Sections 2.3 and 2.4 give details about the concrete system and simulation we are working with. Finally, in section 3 we show the results of our quantitative and visual analysis.

2. METHODS

In this section we describe the two reconstruction methods that we implemented and compared.

Medical Imaging 2009: Physics of Medical Imaging, edited by Ehsan Samei, Jiang Hsieh,
Proc. of SPIE Vol. 7258, 72580T · © 2009 SPIE
CCC code: 1605-7422/09/$18 · doi: 10.1117/12.811118

2.1 Blind Motion-Compensated Reconstruction

In this section, we propose a combined framework of reconstruction and motion estimation. The motivation behind this new approach is to find the best possible fit of image and motion to the measured data. We call our approach "Blind Motion-Compensated Reconstruction" (BMCR)

2.1.1 Model

In (motion-free) PET, the relationship between measured data g and the image f is often approximated by the linear equation

$$g(a) = \int H(a, \boldsymbol{x}) f(\boldsymbol{x}) \, d\boldsymbol{x} \quad . \tag{1}$$

The image is a function $f : \mathbb{R}^3 \mapsto \mathbb{R}$ that maps from a point in three dimensional space to an intensity value. $H : \mathbb{R} \times \mathbb{R}^3 \mapsto \mathbb{R}$ is called the system matrix and totally depends on the underlying physical PET system. $g : \mathbb{R} \mapsto \mathbb{R}$ represents the measurement vector.

In case of subject motion, we model this relationship as

$$\int g(a, t) \, dt = \int H(a, \boldsymbol{x}) \int f(\boldsymbol{\varphi}(\boldsymbol{x}, \boldsymbol{p}(t)) \, dt \, d\boldsymbol{x} \quad . \tag{2}$$

The motion is represented by a function $\boldsymbol{\varphi}$ according to

$$\boldsymbol{\varphi}(\boldsymbol{x}, \boldsymbol{p}(t)) = \begin{pmatrix} c_3 & -s_3 & 0 \\ s_3 & c_3 & 0 \\ 0 & 0 & 1 \end{pmatrix} \begin{pmatrix} 1 & 0 & 0 \\ 0 & c_2 & -s_2 \\ 0 & s_2 & c_2 \end{pmatrix} \begin{pmatrix} c_1 & -s_1 & 0 \\ s_1 & c_1 & 0 \\ 0 & 0 & 1 \end{pmatrix} \begin{pmatrix} x_1 \\ x_2 \\ x_3 \end{pmatrix} + \begin{pmatrix} p_4(t) \\ p_5(t) \\ p_6(t) \end{pmatrix} \quad , \tag{3}$$

with $c_i = \cos(p_i(t))$ and $s_i = \sin(p_i(t))$. The function $\boldsymbol{p}(t) = (p_1(t), p_2(t), p_3(t), p_4(t), p_5(t), p_6(t))^\mathsf{T}$ encapsulates the respective rotation/transformation parameters ($p_1(t), p_2(t)$ and $p_3(t)$ represent rotation parameters and $p_4(t), p_5(t)$ and $p_6(t)$ translation parameters) at time t.

2.1.2 Optimization Framework

We design an objective function

$$\mathcal{J}[f, \boldsymbol{p}] = \mathcal{D}[f, \boldsymbol{p}] + \alpha \, \mathcal{P}[f] + \beta \, \mathcal{M}[\boldsymbol{p}] + \gamma \, \mathcal{S}[\boldsymbol{p}] \quad , \tag{4}$$

that depends on the image f and the motion parameters $\boldsymbol{p}$ and is subject to minimization. The cost functional is designed such that it is minimal for a realistic pair of image f^* and motion $\boldsymbol{p}^*$.

$\mathcal{D}$ is the most important ingredient in our objective functional and assures that the pair f and $\boldsymbol{p}$ fits well to the physical model:

$$\mathcal{D}[f, \boldsymbol{p}] = \frac{1}{2} \iint e_{ta}^2[f, \boldsymbol{p}] \, da \, dt \tag{5}$$

with

$$e_{ta}[f, \boldsymbol{p}] = \int H(a, \boldsymbol{x}) f(\boldsymbol{\varphi}(\boldsymbol{x}, \boldsymbol{p}(t))) \, d\boldsymbol{x} - g(a, t) \quad . \tag{6}$$

Optimization just of $\mathcal{D}$ is an ill-posed problem. There is an infinite number of combinations of f's and $\boldsymbol{p}$'s which bring $\mathcal{D}$ exactly down to zero. However, the vast majority is physically not meaningful. In the next two sections we will discuss several regularization terms in order to encourage physically meaningful solutions.

Without any constraint on the image, optimization of $\mathcal{D}$ will overfit the measured data and usually results in highly noisy images. In order to avoid this, we use the total variation (TV)[4] term

$$\mathcal{P}[f] = \int |\nabla f(\boldsymbol{x})| \, d\boldsymbol{x} \quad . \tag{7}$$

TV is widely and successfully used in the image processing community for stabilizing ill-posed problems by encouraging piecewise smooth images. It is usually preferred over other smoothing terms due to its edge preserving characteristics.

Like for the image, we make use of regularization for the motion since there is an infinite number of pairs of image and motion parameters that minimize $\mathcal{D}$:

Let $(f^*, \boldsymbol{p}^*)$ be a pair of image and motion parameters that minimize $\mathcal{D}$. Then, also every other pair $(f^{**}, \boldsymbol{p}^{**})$ satisfying $f^{**}(\boldsymbol{\varphi}(\boldsymbol{x}, \boldsymbol{p}^{**}(t))) = f^*(\boldsymbol{\varphi}(\boldsymbol{x}, \boldsymbol{p}^*(t)))$ is a minimizer of $\mathcal{D}$. An infinite number of such pairs $(f^{**}, \boldsymbol{p}^{**})$ can be constructed as follows: For any arbitrary but constant parameter vector $\hat{\boldsymbol{p}}$, define $\boldsymbol{p}^{**}(t)$ such that $\varphi(\boldsymbol{x}, \boldsymbol{p}^{**}(t)) = \varphi(\varphi(\boldsymbol{x}, \boldsymbol{p}^*(t)), \hat{\boldsymbol{p}})$. (A concatenation of two rigid transformations $\boldsymbol{\varphi}$ is again a rigid transformation and can therefore be represented by a suitable parameter vector $\boldsymbol{p}^{**}(t)$.) Then define $f^{**} : \boldsymbol{x} \mapsto f^*(\varphi^{-1}(\boldsymbol{x}, \hat{\boldsymbol{p}}))$. (Rigid transformations are invertible.) Then $f^{**}(\varphi(\boldsymbol{x}, \boldsymbol{p}^{**}(t))) = f^*(\varphi^{-1}(\varphi(\boldsymbol{x}, \boldsymbol{p}^{**}(t)), \hat{\boldsymbol{p}})) = f^*(\varphi^{-1}(\varphi(\varphi(\boldsymbol{x}, \boldsymbol{p}^*(t)), \hat{\boldsymbol{p}}), \hat{\boldsymbol{p}})) = f^*(\varphi(\boldsymbol{x}, \boldsymbol{p}^*(t)))$.

We will restrict these unwanted degrees of freedom by discouraging extensive motion with a minimal motion term:

$$\mathcal{M}[\boldsymbol{p}] = \frac{1}{2} \iint |\boldsymbol{\varphi}(\boldsymbol{x}, \boldsymbol{p}(t)) - \boldsymbol{x}|^2 \, d\boldsymbol{x} \, dt \tag{8}$$

Additionally, we discourage huge inter-frame movements:

$$\mathcal{S}[\boldsymbol{p}] = \frac{1}{2} \iint \left| \frac{\partial}{\partial t} \boldsymbol{\varphi}(\boldsymbol{x}, \boldsymbol{p}(t)) \right|^2 \, d\boldsymbol{x} \, dt \quad . \tag{9}$$

We optimize $\mathcal{J}$ by calculating the respective functional derivatives and use them for a gradient descent algorithm with variable stepsize.

2.2 Registration and Fusion of Reconstructed Frames

This approach is implemented for being able to compare BMCR to a state-of-art method. It consists of the following steps:

- Divide the data into different time frames.
- Reconstruct each frame individually using any standard reconstruction method. We use the ML-EM algorithm with 30 iterations.
- Register each reconstructed frame to a reference frame (we use the first frame)
- Fuse images: we simply fused the resulting reconstructed frames by summing them up in image space.

For image registration, we optimize a cost function by the downhill simplex method of Nelder and Mead.[5] As cost function we use the negative Pearson product-moment correlation coefficient:

$$\mathcal{C}[\boldsymbol{x}, \boldsymbol{y}] = -\frac{\boldsymbol{x} \cdot \boldsymbol{y}}{\|\boldsymbol{x}\| \, \|\boldsymbol{y}\|} \quad , \tag{10}$$

where $\boldsymbol{x}$ is a vector which represents the data of the first image and $\boldsymbol{y}$ is a vector which represents the data of the second image in the same order as the first one. Both vectors are centered (that is, shifted such that their mean is zero) when applied to the formula.

Note that some authors use more sophisticated methods for fusing the data. For example, Rubio-Guivernau *et al.* and Quiao *et al.* apply a special motion compensating reconstruction algorithm based on the motion information gathered from the registration.[2,3] We justify the use of a simple fusion method (summation of registered frames) by noting that the knowledge of the registration step which gives rise to the motion information is the crucial step for motion compensation.

2.3 Scanner

We work with a fictitious one-ring PET system and a Siemens Biograph 16 where only one of the 24 rings is used.

2.3.1 Ficticious One-Ring PET

The ring consists of ten crystal blocks and each block of one hundred crystals. The crystals are aligned linearly within each block. The field of view is a 50×50 image which is centered within the ring. The system matrix is calculated with Siddon's algorithm.[6]

2.3.2 Siemens Biograph 16

We simulate one of 24 rings of the Siemens Biograph 16. The ring consists of 48 blocks and each block of 8 crystals. The field of view is a 60×60 image which is centered within the ring. The system matrix is calculated with Scheins's algorithm.[7]

2.4 Simulations

We simulate data acquisition for several objects and levels of statistical noise. For each object and noise level, the measured data $g(\cdot, t)$ in time frame t is generated according to the following steps:

- Application of a smooth rigid transformation (a sinusoidal movement of one period in x and y direction combined with a rotation of constant speed of up to 60 degrees).
- Projection of the transformed image to the measurement space by multiplication with the system matrix. This yields the expected values of the number of counts for each LOR.
- Generation of Poisson random numbers according to the previously generated expected values and the measurement time.

Since we want to focus on motion artifacts, we do not simulate physical effects like attenuation and accidental/scattered coincidences. Accordingly, the only source of degradation of image quality is due to motion and statistical noise.

For simulation, we chose 100 time frames. For reconstruction, 10, 25 and 50 frames are used. We chose less reconstruction frames than simulation frames in order to provide a more realistic scenario in which motion can be present even within a time frame. Data of several simulation frames is combined into one reconstruction frame (10 for 10 reconstruction frames, 4 for 25 reconstruction frames and 2 for 50 reconstruction frames).

3. RESULTS AND DISCUSSION

We compare the BMCR algorithm to (a) the ML-EM method and (b) the previously described RFRF method. Furthermore, we analyze the relation between the number of iterations and the image quality of the reconstructed image.

3.1 Comparison of BMCR to ML-EM

Figure 1 shows applications of the BMCR algorithm for an MR-based brain and an artificial ring. We compare the BMCR algorithm applied to motion-*contaminated* data with a standard Maximum-Likelihood Expectation-Maximization (ML-EM) reconstruction applied to (a) motion-*contaminated* data and (b) motion-*free* data.

As expected, BMCR on motion-contaminated data is visually clearly superior to ML-EM reconstruction on motion-contaminated data (compare first row with rows two to four). However, BMCR reconstruction on motion-contaminated data can even get close to a ML-EM reconstruction on motion-free data (e.g. compare last row to second row for medium statistics). In this example, the number of reconstruction frames does not make a big difference.

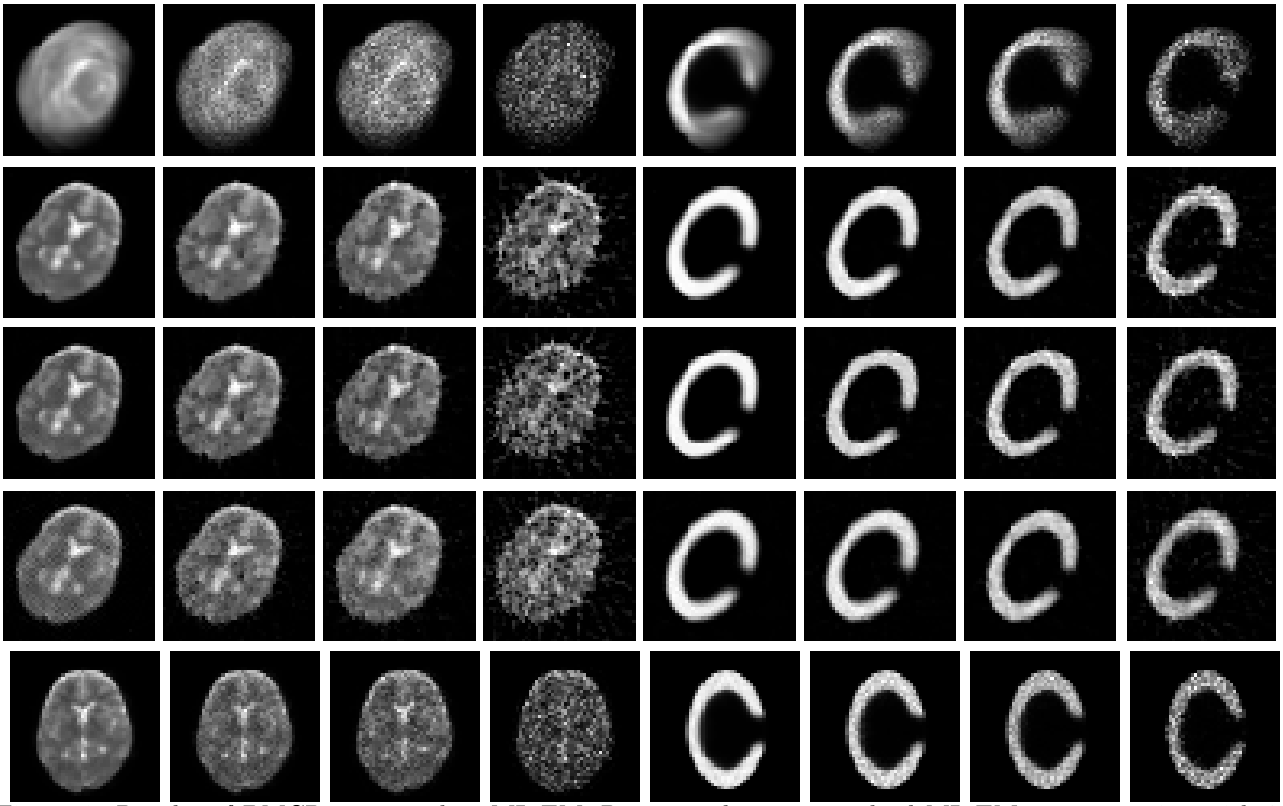

Figure 1: Results of BMCR compared to ML-EM. Row one shows a standard ML-EM reconstruction with 30 iterations of motion-contaminated data. Rows two to four show a BMCR reconstruction for motion-contaminated data with (2) 50 reconstruction frames, (3) 25 reconstruction frames and (4) 10 reconstruction frames. Row five shows a standard ML-EM reconstruction with 30 iterations of motion-free data for comparison reasons. Columns left to right: (1) perfect statistics, (2) high statistics, (3) medium statistics and (4) low statistics. Same for columns five to eight.

3.2 Comparison of BMCR to RFRF

Figure 2 shows a visual comparison between BMCR and the RFRF approach. We compare the (positive!) Pearson product-moment correlation coefficient between the original image and the reconstructed images. Different levels of statistical noise (expressed by the number of counts) are evaluated. The correlation coefficient can reach a maximum of 1 - however, even in a motion-free scenario it could not be expected that this maximum can be reached by any reconstruction method since the measured data is suffering from statistical noise.

By comparing row two (BMCR) with row three (RFRF) of Figure 2 it can be clearly seen that BMCR reconstructions are visually superior. Note that BMCR was stopped after 120 iterations for each noise level.

Figure 3 shows a quantitative evaluation of the same data and confirms the visual impression that BMCR is significantly superior to the RFRF approach.

3.3 Relation Between Number of Iterations and Image Quality

Figure 4 shows images reconstructed by BMCR for different numbers of iterations. Figure 5 gives a quantitative evaluation of the image quality with respect to the number of iterations for several levels of statistical noise. In general, image quality increases with the number of iterations. However, for higher noise levels, it decreases slowly after 40 to 60 iterations.

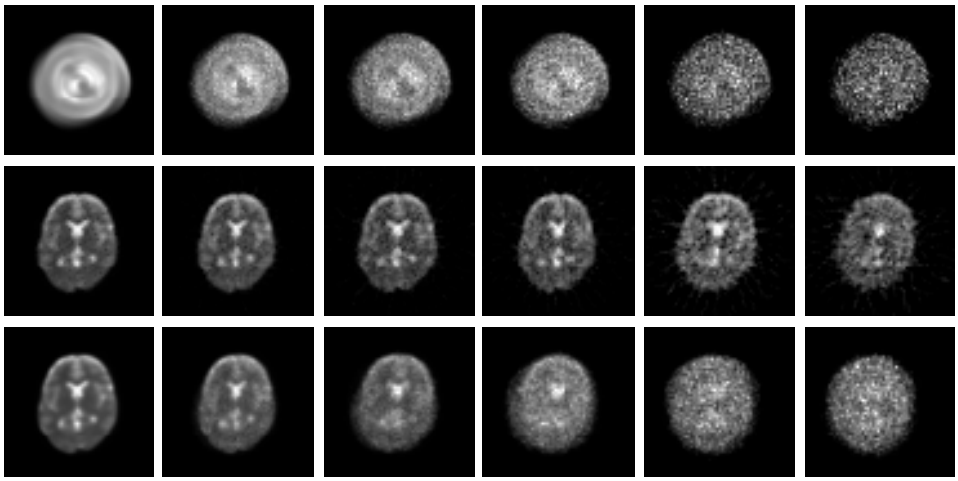

Figure 2: Results of BMCR compared to the RFRF approach. The first row shows a standard ML-EM reconstruction with 30 iterations of motion-contaminated data. The second row shows a BMCR reconstruction for motion-contaminated data. Row three shows an RFRF reconstruction. Columns left to right: (1) infinite number of counts, (2) $\approx$ two million counts, (3) $\approx$ one million counts, (4) $\approx$ 600.000 counts, (5) $\approx$ 200.000 counts and (6) $\approx$ 140.000 counts.

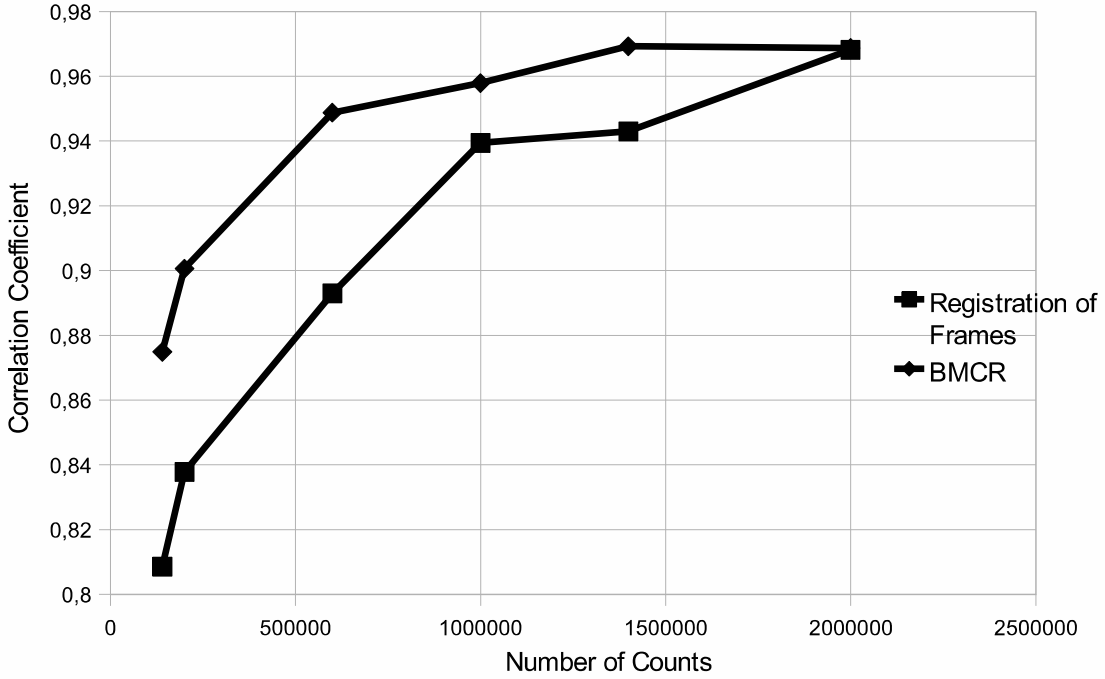

Figure 3: Results of BMCR compared to RFRF approach

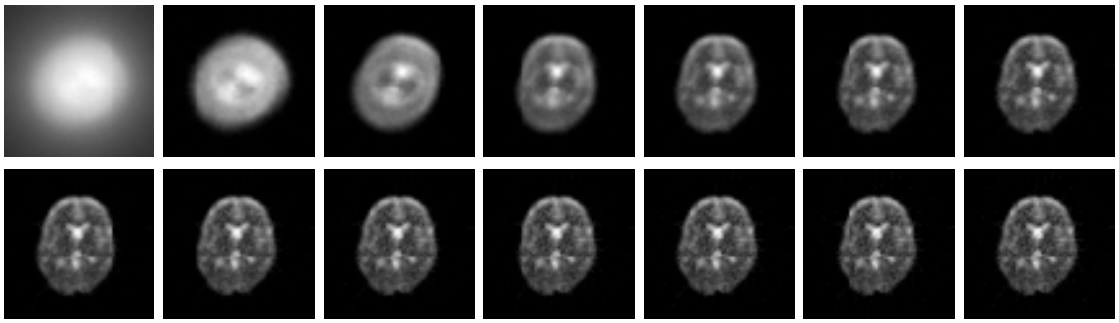

Figure 4: BMCR for one million counts: image at left-top is reconstruction after first iteration, then the number of iterations increases by ten from left to right and top to bottom.

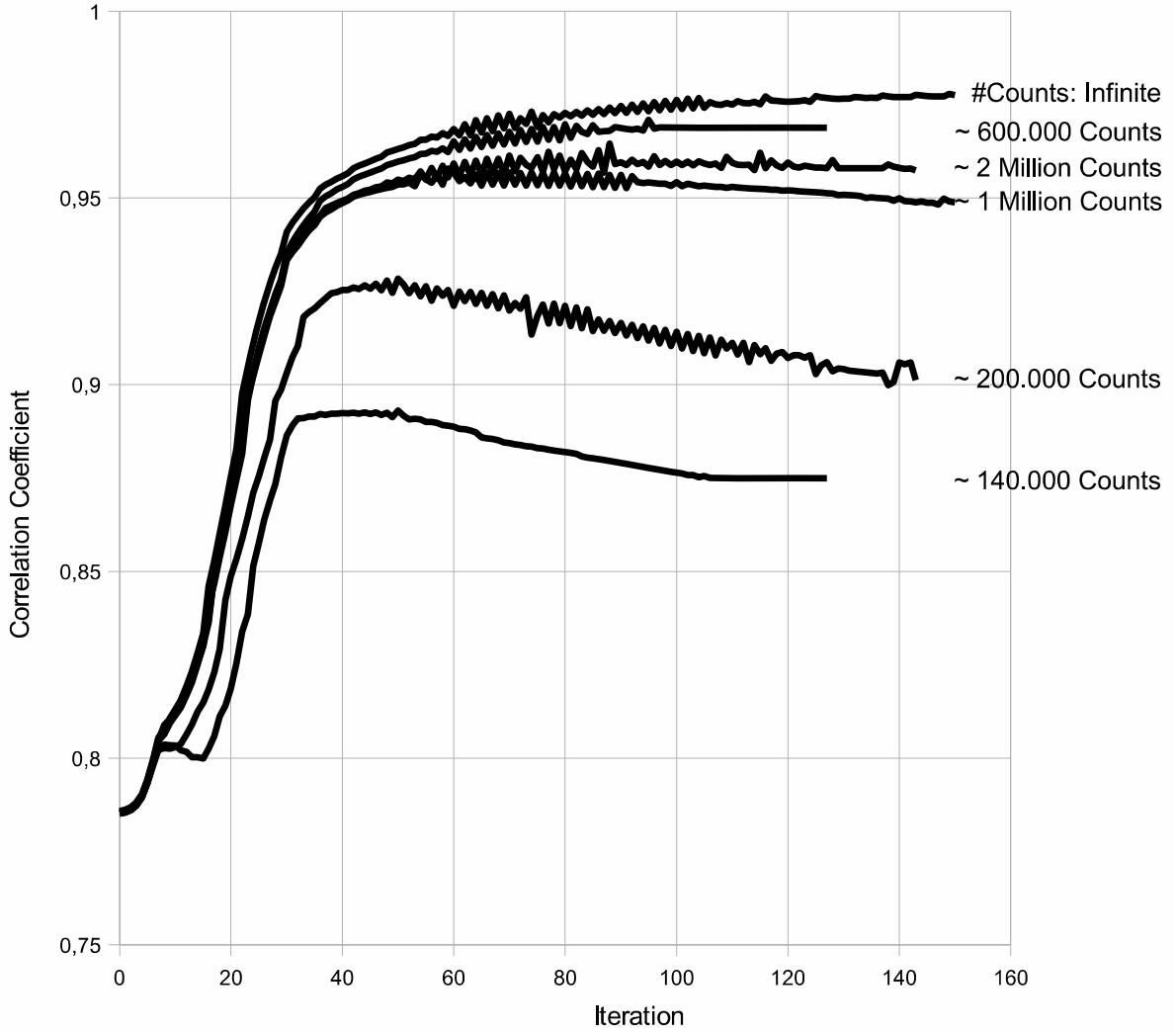

Figure 5: Comparison of reconstructions with BMCR to original image for different number of counts. As comparison measure the correlation coefficient is used.

4. CONCLUSION AND FUTURE WORK

We present an algorithm (BMCR) for combined reconstruction and motion estimation for PET. BMCR is an intrinsic algorithm and thus is able to recover both image and motion just from the data, without the need of external motion tracking. First results are promising even for very short and therefore low statistics time frames. We compare BMCR to a state-of-the-art intrinsic method and show that BMCR provides a superior reconstruction with respect to the image quality.

Future work includes experiments on real data and automatic retrieval of the regularization parameters.

REFERENCES

[1] Klein, G. J., Reutter, B. W., and Huesman, R. H., "4d affine registration models for respiratory-gated PET," in [*Nuclear Science Symposium Conference Record, 2000 IEEE*], **2**, 41–15 (2000).

[2] Rubio-Guivernau, J. L., Ledesma-Carbayo, M. J., Lamare, F., Ortuno, J. E., Guerra, P., Visvikis, D., Santos, A., and Kontaxakis, G., "Respiratory motion correction in PET with super-resolution techniques and non-rigid registration," in [*Nuclear Science Symposium Conference Record, 2007. NSS '07. IEEE*], **5**, 3560–3563 (Oct./Nov. 2007).

[3] Qiao, F., Pan, T., Jr, J. W. C., and Mawlawi, O. R., "A motion-incorporated reconstruction method for gated pet studies," *Physics in Medicine and Biology* **51**(15), 3769–3783 (2006).

[4] Rudin, L. I., Osher, S., and Fatemi, E., "Nonlinear total variation based noise removal algorithms," *Physica D* **60**, 259–268 (1992).

[5] Nelder, J. A. and Mead, R., "A simplex method for function minimization," *The Computer Journal* **7**, 308–313 (January 1965).

[6] Siddon, R. L., "Fast calculation of the exact radiological path for a three-dimensional ct array.," *Med Phys* **12**(2), 252–255 (1985).

[7] Scheins, J. J., Boschen, F., and Herzog, H., "Analytical calculation of volumes-of-intersection for iterative, fully 3-d PET reconstruction," *IEEE Transactions on Medical Imaging* **25**, 1363–1369 (Oct. 2006).